Flame Burning Speeds and Combustion Characteristics of Undiluted and Nitrogen Diluted Hydrogen-Nitrous Oxide Mixtures

S.P.M. Bane[*,a], R. Mével[a,b,c], S.A. Coronel[a], J.E. Shepherd[a]

[a]*Graduate Aerospace Laboratories, California Institute of Technology*
1200 E. California Blvd., MC 205-45
Pasadena, California 91125, USA
[b]*Institut de Combustion, Aérothermique, Réactivité et Environnement (ICARE)*
Centre National de la Recherche Scientifique (CNRS), Orléans, France
[c]*University of Orléans, France*

Abstract

In the present study, some explosive properties of undiluted and nitrogen diluted H_2-N_2O mixtures were characterized. Laminar burning speeds and the explosion-induced pressure rises were determined experimentally for a range of mixture equivalence ratios ($\phi = 0.15 - 1.0$), dilutions ($0 - 55\%$ N_2), and initial pressures ($20 - 80$ kPa). The measured burning speeds were used to validate laminar burning speed computations using a detailed chemical kinetic mechanism. The computations were then used to estimate burning speeds at high initial pressure and low dilution conditions that could not be measured experimentally. The results demonstrate that hydrogen-nitrous oxide mixtures exhibit laminar burning speeds as large as 350 cm/s and pressure rise coefficients (K_g) as large as 35 MPa·m/s. Also, flames in lean mixtures are shown to be highly unstable which can lead to flame acceleration and possible deflagration-to-detonation transition.

Key words: Hydrogen, Nitrous oxide, Flame speed

[*]Corresponding author: sallym@caltech.edu
ph: +1 (626) 395-3163
fax: +1 (626) 395-2900

1. Introduction

The Hanford site, located in south central Washington state, was opened in 1943 as part of the Manhattan Project. It was used for more than 40 years mainly to produce plutonium for the United States' nuclear weapons arsenal, playing a crucial role at the end of World War II and during the Cold War. The plutonium production at Hanford also led to the largest amount of localized nuclear waste in the United States. Since the cessation of plutonium production in the late eighties, the Hanford site has been in a waste cleanup phase which will extend over several decades [1, 2]. It has been determined that the stored waste continuously generates gaseous compounds that form mixtures of H_2, N_2O, O_2, N_2, NH_3 and CH_4 [3]. Therefore, in addition to safety concerns involved with handling radioactive material, the hazard posed by accidental explosions in these gas mixtures must also be considered. Mixtures of hydrogen and nitrous oxide pose the most severe hazard [4], and if accidentally ignited, could lead to failure of the pipelines due to the explosion pressure rise or deflagration-to-detonation transition (DDT).

The explosive properties of H_2-N_2O have been characterized with numerous studies on ignition delay times [5–7], detonation cell size [8, 9], and flammability limits [4, 10, 11]. Recently, Liang et al. [12] demonstrated that, at ambient conditions, flames in hydrogen-nitrous oxide mixtures with low concentrations of H_2 can undergo DDT in relatively short distances. Fewer studies have been performed to determine burning speeds in H_2O-N_2O mixtures. The burning speed is used in theoretical modeling of the pressure-time history inside a vessel or piping system, which is important to consider during the design process [13]. Rodriguez [13] cites five studies where experimental values of the laminar burning speed for H_2-N_2O mixtures were obtained, as summarized in Table 1. However, in four of the studies the data were obtained for only one, very low initial pressure (70 Torr/9.33 kPa) [14–17] and no information is known about the initial pressure or temperature in the results from Kozachenko and Skachkov [18]. In the 1960s, Dixon-Lewis et al. [19] obtained burning speed data for a limited range of H_2-N_2O-N_2 mixtures using a flat flame burner technique. Recently, Powell et al. [20] obtained burning speed data for mixtures with high nitrogen dilution at one initial pressure (0.80 atm/81.06 kPa), and Mével

et al. [21] presented data for mixtures diluted with 60% argon at 1 atm (101.3 kpa) initial pressure. Despite these substantial contributions by previous studies, there remain large gaps in the data for burning speeds for both diluted and undiluted H_2-N_2O mixtures over a range of compositions and initial pressures. Therefore, a more complete characterization of the flame behaviors, including laminar flame burning speeds and explosion pressures, is needed for risk assessment at Hanford and other industrial sites.

Table 1: Laminar burning speeds obtained experimentally in previous studies, as given in [13].

ϕ	S_L (cm/s)	p_0 (Torr)/9.33 (kPa)	T_0 (K)	Source
0.11	22	70	335	[14]
0.176	30	70	334	[15]
0.176	38			[18]
0.25	48	70	334	[15]
0.25	89	70	335	[16]
0.25	87			[18]
0.429	126	70	334	[15]
0.429	186			[18]
0.923	385	70	335	[14]
1.0	390	70	335	[17]
1.0	404	70	334	[15]
1.0	379	70	335	[16]
1.083	398	70	335	[14]
1.128	397	70	335	[17]
1.222	385			[18]
1.5	371	70	335	[14]
2.333	272	70	335	[14]

The objective of the present study is to obtain a more complete characterization of the laminar burning speeds and explosion pressures for both undiluted and

nitrogen-diluted H_2-N_2O mixtures. Experiments were performed for a range of mixture equivalence ratios, dilution levels, and initial pressures to study the effect on the flame burning speed and explosion pressure. The burning speeds were then calculated using one-dimensional flame computations with detailed chemistry and compared with the experimental results. Once the flame model was validated using the experimental data, it could then be used to calculate laminar burning speeds of undiluted mixtures at initial pressures of one to three atmospheres, which are the conditions of interest for risk assessment and where the present data sets are most lacking.

2. Experiments

2.1. Experimental Method

The experiments were performed in a stainless steel cylindrical vessel approximately 30 cm in height and diameter. Two parallel flanges were used to mount the electrodes for the ignition system. The flames were ignited using a capacitive spark discharge circuit described in detail in [22]. The ignition system generated a spark with energy on the order of 300 mJ across a 2 mm spark gap, and the electrodes were made out of tungsten wire 0.38 mm in diameter.

Two other parallel flanges held BK7 glass windows approximately 11.7 cm in diameter to allow for schlieren visualization of the flame propagation. A high-speed camera was used to record the schlieren visualization at a rate of 10,000 to 85,000 frames per second with resolutions of 800 x 800 and 256 x 256, respectively.

Before each experiment, the vessel was evacuated to less than 10 Pa and then the gases were filled using the method of partial pressures. A static pressure manometer was used to measure the gas pressure inside the vessel to within 0.01 kPa, allowing for extremely precise determination of the mixture composition. The gas was thoroughly mixed using a magnetically-driven fan mixer and was allowed to come to rest by waiting a fixed amount of time before igniting the mixture. The pressure evolution in the vessel was measured using a piezoresistive pressure transducer.

4

2.2. Flame Burning Speed Measurement

To derive the laminar burning speed from spherically expanding flame experiments, it is necessary to use a correction to account for the stretch effect. According to asymptotic analysis [23–25], the burning speed stretch correction in the low stretch rate regime is conventionally given by

$$S_L = S_L^0 - L \cdot K ,\tag{1}$$

where S_L is the stretched laminar burning speed, S_L^0 is the unstretched laminar burning speed, L is the Markstein length, and K is the flame stretch rate. Assuming an ideal spherical flame, the burning speed is related to the spatial flame velocity, V_S, by

$$S_L = \frac{V_S}{\sigma} ,\tag{2}$$

where $\sigma = \rho_u/\rho_b$ is the gas expansion ratio with ρ_u and ρ_b as the densities of the unburned and burned gases, respectively. Substituting Equation 2 into Equation 1 gives

$$V_S = V_S^0 - \sigma L K ,\tag{3}$$

where V_S^0 is the unstretched spatial flame velocity.

The general expression for the stretch rate of a spherical flame is [24, 26, 27]

$$K = \frac{1}{A}\frac{dA}{dt}\tag{4}$$

where A is the surface area of the flame front. In the case of a spherically expanding flame, the stretch rate can be calculated [26–30] as

$$K = \frac{1}{A}\frac{dA}{dt} = \frac{1}{R_f^2} \cdot \frac{dR_f^2}{dt} = \frac{2}{R_f} \cdot \frac{dR_f}{dt} = 2 \cdot \frac{V_S}{R_f}\tag{5}$$

with $V_S = dR_f/dt$. Combining Equation 3 and Equation 5 and integrating with respect to time results in an expression for the unstretched spatial flame velocity as a function of time and flame radius,

$$V_S^0 \cdot t = R_f + 2\sigma L \cdot ln\left(R_f\right) + C\tag{6}$$

where C is an integration constant.

Calculating a least squares fit to the experimentally-measured temporal evolution of the flame radius and extrapolating back to zero stretch [27, 28] allows one to obtain the unstretched laminar burning speed, S_L^0, by dividing the unstretched spatial velocity, V_S^0, by the expansion ratio.

The expansion ratio for each mixture was calculated using an equilibrium solution [31] for a constant-pressure explosion to obtain the burned gas density. The maximum pressure rise during the experimental measurement is less than 2% of the initial pressure, so that all of the measurements and analysis of burning speed take place at essentially the initial pressure.

Particular care has to be taken when deriving the flame speed and burning speed from enclosed vessel experiments. First, the visualization of the flame front must be done using a high sampling rate to obtain a sufficient number of frames. It is also important that the flame propagates spherically with negligible buoyancy and that the stretch rate is low so that the assumptions of the asymptotic theory remain valid. Cellular flames cannot be used to derive the burning speed because in that case a simple relation does not exist to calculate the flame surface area from its radius. Additionally, the first few visual frames have to be removed from the analysis due to the flame accelerating effect of the inflammation energy at ignition. Finally, the flame speed measurement must be limited to the first few centimeters of flame front propagation so that there is no influence of the finite size of the vessel due to adiabatic compression of the fresh mixture induced by the flame expansion [32].

To perform an objective quantitative analysis of the flame visualization, a MATLAB routine was used to obtain the flame radius as a function of time and derive V_S^0 from the schlieren images as described in detail in Mével et al. [21]. A background image is first obtained and then removed from the subsequent images. The edge of the expanding flame is detected using a built-in MATLAB function, and an ellipse is fitted to the flame front to obtain the radius. Then, a least-squares regression is performed on the data to obtain the unstretched flame burning speed and the Markstein length and the uncertainties. The uncertainties of the laminar burning speed and the Markstein length are approximately 6 and 20%, respectively.

3. Flame Burning Speed Calculation

Laminar burning speeds were calculated using the one-dimensional freely propagating flame code in Cantera. The detailed kinetic model of Mueller et al. [33] was used in the flame code. It is composed of 122 reversible reactions and 24 chemical species, and the thermodynamic data of Mueller [33] and the transport parameters from Konnov [34] were used in the mechanism. The kinetic model has been validated against flow reactor measurements for H_2-N_2O mixtures and burning speed data [32].

4. Results and Discussion

4.1. Laminar Flame Burning Speeds

Experimental burning speed measurements have been performed at ambient temperature for both undiluted and nitrogen-diluted H_2-N_2O mixtures. For the undiluted mixtures, the effect of equivalence ratio on the burning speed was investigated by varying the equivalence ratio from $\phi = 0.15$ to $\phi = 0.70$. At higher equivalence ratios the stretch rate is very high (> 2000 s^{-1}) during the majority of the observation time, and the asymptotic theory described in Section 2.2 is valid only at low stretch rates (~ 2000 s^{-1} and lower). Also, the initial pressure was fixed at 20 kPa for all the undiluted mixtures due to the very fast onset of cellular instabilities at higher initial pressures. For the nitrogen-diluted mixtures, the effect of both the initial pressure and nitrogen content was investigated. Tests with dilution were performed with initial pressures of 20 to 80 kPa and with N_2 molar concentration of 20 to 55%.
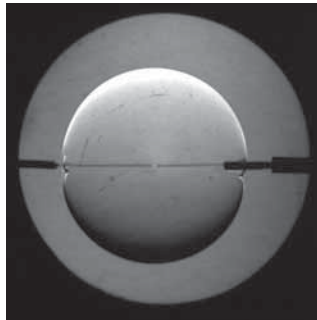
An example of a schlieren image sequence of flame propagation in a stoichiometric H_2-N_2O mixture with 40% N_2 dilution is shown in Figure 1. The initial temperature and pressure were 298 K and 60 kPa, respectively, and the camera framing rate was 18,000 images per second. After ignition by the spark, the flame develops and propagates as a smooth surface. The initial perturbations to the flame front induced by the electrodes do not grow because of the stabilizing effects of diffusion and flame stretch. This type of flame propagation with a smooth flame surface is well-suited for deriving a laminar burning speed.
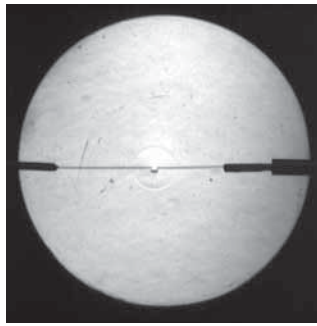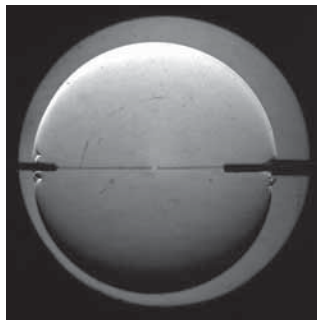
(a) t=0 ms
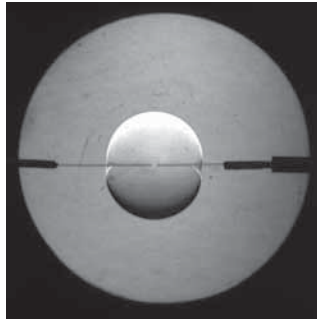
(b) t=1.2 ms

(c) t=2.3 ms

(d) t=3.1 ms

Figure 1: Example of a schlieren image sequence of flame propagation in a stoichiometric H_2-N_2O-N_2 mixture with 40% N_2 dilution and initial pressure of 60 kPa. The field of view has a diameter of approximately 11.7 cm.

The results for the measured laminar burning speeds for undiluted mixtures as a function of equivalence ratio are shown in Figure 2 and given in Table 1 in the Electronic Supplementary Material. The initial temperature was 298 K and the initial pressure was 20 kPa for these experiments. The laminar burning speed increases continuously with ϕ and varies by an order of magnitude, from 19 cm/s for $\phi = 0.15$ to 260 cm/s for $\phi = 0.7$. The burning speeds calculated using the detailed kinetic model are also shown in Figure 2 as the solid line. The average percentage deviation between the measured and computed burning speeds was 14%, with a minimum deviation of 2% for $\phi = 0.40$ and 42% for the leanest mixture, $\phi = 0.15$. Significant errors in model predictions are generally observed for very lean mixtures and can be due to several different issues. First, for very low burning speeds like those in fuel-lean mixtures, the flame temperature is low, and there may be uncertainties in the mechanism rate constants at low temperature or missing low-temperature chemical pathways. Also, in lean hydrogen-based mixtures the onset of instabilities occurs very early on in the flame propagation, resulting in a higher burning speed. Finally, flames in lean mixtures can be affected by buoyancy, causing the flame front to no longer be round. Therefore, while the flame model significantly underpredicts the burning speed for very lean mixtures, the calculated burning speeds agree with the measured data to within 10% for mixtures away from the lean limit.
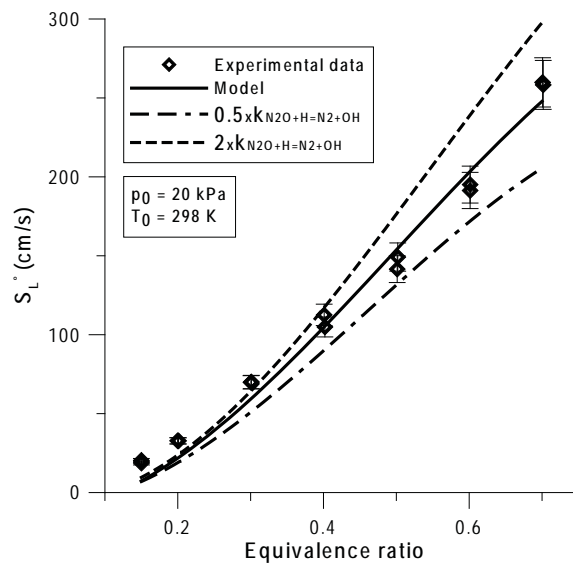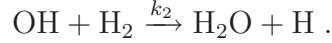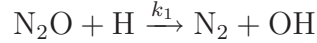
Figure 2: Experimental and predicted values for the laminar burning speed versus equivalence ratio for undiluted H_2-N_2O mixtures at 20 kPa initial pressure.

For freely propagating flames in H_2-N_2O mixtures, the energy release rate, and thus the flame burning speed, is primarily controlled [21] by the linear reaction chain:

$$N_2O + H \xrightarrow{k_1} N_2 + OH$$

$$OH + H_2 \xrightarrow{k_2} H_2O + H .$$

To confirm the important effect of the rate constant of the very exothermic first reaction, calculations have been performed for a higher and lower value of the reaction rate parameter k_1: $k = 2k_1$ and $k = 0.5k_1$. The results of these computations are also shown in Figure 2 as dashed and dashed-dotted lines. The influence of the $N_2O + H \rightarrow N_2 + OH$ reaction on the burning speed increases with the equivalence ratio. For $\phi = 0.7$, significant differences in the predicted burning speed are observed when modifying the rate constant; increasing the rate constant to $2k_1$ results in a 16% increase in the burning speed, and decreasing it to $0.5k_1$ results in an 18% decrease. For very lean mixtures, the influence of the $N_2O + H \rightarrow N_2 + OH$ reaction is negligible, likely due to the very low H atom content.

The results for stoichiometric H_2-N_2O-N_2 mixtures with varying N_2 dilution are shown in Figure 3 and given in Table 2 in the Electronic Supplementary Material. The initial temperature was 298 K and the initial pressure was varied from 20 to 80 kPa. Instead of burning speed, the mass flow rate per area of fresh gas, $S_L^0 \cdot \rho_{ini}$, through the flame front is plotted as a function of the N_2 dilution to clearly distinguish between cases at different pressures. At a given N_2 dilution, no significant variation of the burning speed was observed when increasing the initial pressure. However, the mass flow rate through the flame increases as the initial pressure increases and the nitrogen dilution decreases. The predictions of the kinetic model are also shown in Figure 3 and given in Table 3 in the Electronic Supplementary Material. The average percentage deviation between the measured and computed burning speeds was 5%, with a minimum and maximum deviation of 0% and 12%, respectively. For stoichiometric mixtures, the influence of the $N_2O + H \rightarrow N_2 + OH$ reaction is very significant, and large variations of the calculated burning speed are induced by modification of the rate constant k_1.
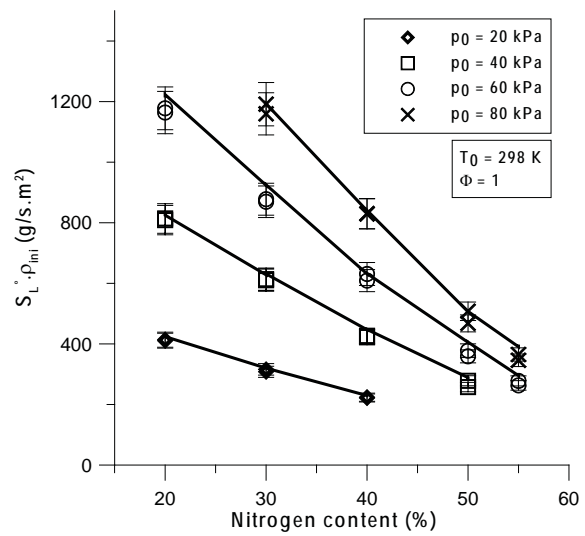
Figure 3: Laminar mass flow rate per unit area through the flame front in H_2-N_2O-N_2 mixtures as a function of nitrogen dilution and initial pressure. Kinetic model predictions are shown as solid lines.

The results demonstrate that burning speeds calculated using a one-dimensional flame model with the detailed chemistry of Mueller et al. [33] are in reasonable agreement with the experimental data. Therefore, the model can be used to calculate flame burning speeds for H_2-N_2O mixtures that have not been investigated experimentally or for conditions that may pose a hazard to test in the laboratory. Two sets of new calculations using the model are shown in Figures 4 and 5. Figure 4 shows calculated laminar burning speeds for a stoichiometric mixture at atmospheric pressure with N_2 dilution ranging from 0 to 70%. Laminar burning speeds for undiluted H_2-N_2O mixtures at 100 kPa and two elevated initial pressures (200 and 300 kPa) are shown in Figure 5. The results of these calculations are also given in Table 4 in the Electronic Supplementary Material. The burning speed drops sharply as the N_2 dilution increases. For example, increasing the dilution to 40% reduces the burning speed by more than a factor of three due to the decrease of the energy content of the mixture and of the flame temperature caused by the nitrogen addition. Figure 5 shows that the burning speed is only slightly affected by increasing the initial pressure from 100 to 300 kPa. Under these conditions, burning speeds as high as 350 cm/s have been calculated. According to the theory of Mallard and Le Châtelier, the pressure dependency of the burning speed is given by

$$S_L \sim p^{(n-2)/2} \tag{7}$$

where n is the global reaction order [35]. Using the method of Bane [36], it was demonstrated that the global reaction orders for H_2-N_2O mixtures are close to $n = 2$, which explains the observed low pressure dependency of the burning speed. The laminar burning speed is a maximum near $\phi = 1.5$. As a first approximation, the burning speed can considered to be proportional to square root of the product of the thermal diffusivity, α, and the time derivative of the reaction progress variable, ξ [35], i.e.,

$$S_L \sim \left(\alpha \frac{\partial \xi}{\partial t} \right)^{1/2} . \tag{8}$$

For H_2-N_2O mixtures, the global reaction rate and adiabatic flame temperature reach maximum values at $\phi = 1$, whereas the thermal diffusivity increases with increasing H_2 concentration. Because of the high diffusivity of hydrogen, the maximum burning

speed is shifted toward a higher equivalence ratio than $\phi = 1$. Further discussion about this phenomenon can be found in Mével et al. [21]. The present results show that calculations such as these can provide important flame burning speed and pressure data for use in safety assessment and design without the necessity of performing experiments.
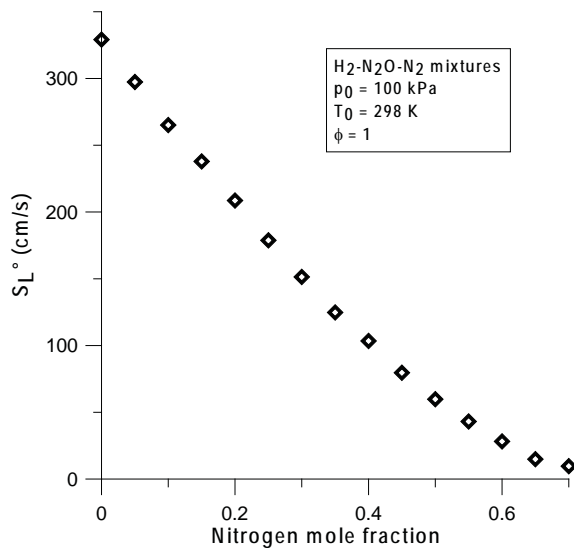
S_L° (cm/s)

300

200

100

0

H$_2$-N$_2$O-N$_2$ mixtures
p_0 = 100 kPa
T_0 = 298 K
ϕ = 1

0   0.2   0.4   0.6

Nitrogen mole fraction

Figure 4: Laminar burning speeds calculated using the mechanism of Mueller et al. [33] for stoichiometric H$_2$-N$_2$O-N$_2$ mixtures with varying N$_2$ dilution.
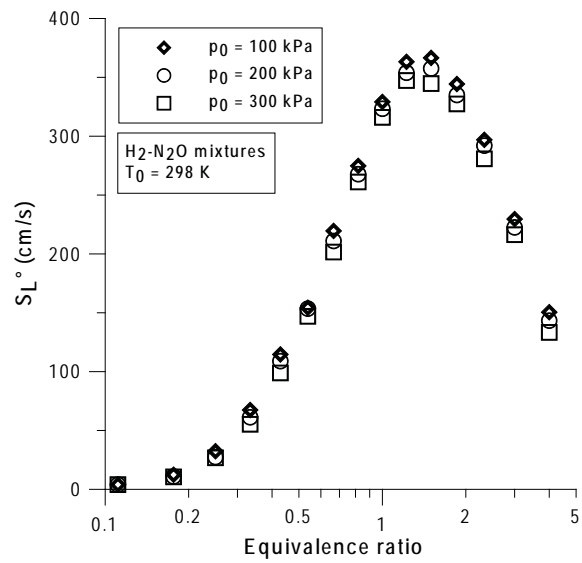
Figure 5: Laminar burning speeds calculated using the mechanism of Mueller et al. [33] for undiluted H_2-N_2O mixtures at initial pressures of 100, 200, and 300 kPa.

4.2. Pressure Signal Analysis

The temporal evolution of the pressure and the peak explosion pressure in the vessel have been examined at ambient temperature for undiluted and nitrogen-diluted H_2-N_2O mixtures. The pressure in the vessel was measured using a piezoresistive pressure transducer as described in Section 2.1. For undiluted mixtures, the effect of the equivalence ratio on the explosion pressure was studied for $\phi = 0.15$ to $\phi = 1$ at two initial pressures, 20 and 40 kPa. For nitrogen-diluted mixtures, the effect of nitrogen content was examined for stoichiometric mixtures for a range of initial pressures (20 to 80 kPa) and N_2 molar concentrations (0 to 55%). However, for $p_0 = 80$ kPa the 0 and 10% N_2 cases were not included due to safety concerns.

The measured peak explosion pressure for stoichiometric mixtures is shown in Figure 6 as a function of nitrogen dilution and initial pressure. As expected, the peak pressure increases as the N_2 concentration decreases due to the increase in the energy content of the mixture with less dilution. Also, the maximum pressure during the explosion increases with higher initial pressures. Over the range of experimental conditions, the ratio of the peak pressure to the initial pressure varied from 8.25 for mixtures with 55% N_2 dilution to 12.4 for undiluted mixtures. The theoretical explosion pressures, calculated using adiabatic constant volume explosion calculations in Cantera, are also shown as solid lines in Figure 6. The measured maximum pressures are 4 to 13% lower than the theoretical values due to heat losses to the vessel walls during the combustion process. The explosion pressure versus time exhibits a very fast rise to a peak pressure, on the order of 8 ms for undiluted mixtures to 65 ms for mixtures with 55% N_2 dilution, followed by an exponential decay. An example of a typical pressure trace is given in Figure 7 for an undiluted H_2-N_2O mixture with $\phi = 0.3$ and initial pressure of 40 kPa. This type of pressure versus time behavior is characteristic of approximately spherical flame propagation. However, it was found that for cases with very sufficiently high dilution or low equivalence ratio, the flame propagation was dominated by buoyancy as observed in previous hydrogen studies [4, 21, 37]. In these cases, the hot products rise and the flame extinguishes with minimal initial downward propagation. Figure 8 shows a series of schlieren images depicting a buoyant flame in a H_2-N_2O-N_2 mixture with 60% N_2 dilution, $\phi = 0.30$,

16

and initial pressure of 100 kPa. The motion of the flame is initially dominated by the buoyancy of the hot, lighter combustion products moving upward and displacing the cold, denser reactants. Therefore, the flame propagates to the top of the vessel, where the upper surface of the flame is extinguished. After an extended time period on the order of 600 ms, the bottom surface of the flame is able to propagate downward. This flame behavior is reflected in the pressure trace, also shown in Figure 7. The pressure rises much more slowly, reaching a low peak pressure and remaining near this pressure over a long period of time (on the order of 3 seconds) as the flame continues to propagate downward. Both adiabatic compression and induced fluid motion of the fresh mixture contribute to this flame behavior. As the flame propagates upward, the pressure in the vessel increases and the fresh gases undergo adiabatic compression. The compression induces heating of the fresh mixture and so the flammability domain is widened and the flame speed increases. Also, as the buoyant flame has sufficient momentum, a downward flow is created after the flame collides with the upper vessel wall. The gravity forces are counteracted, allowing the flame to propagate downward.
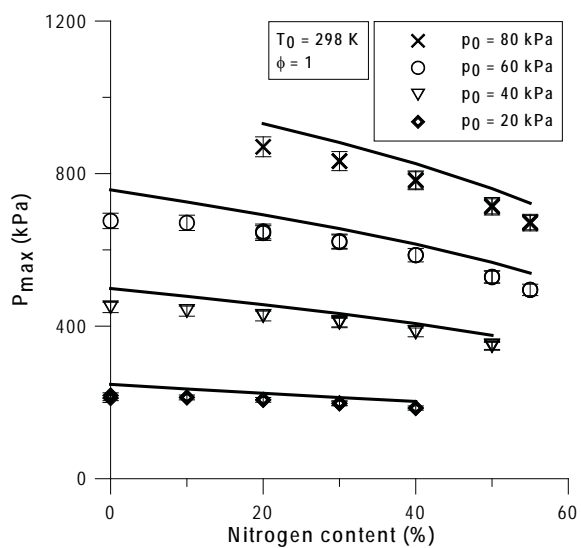

Figure 6: Peak explosion pressure for stoichiometric H_2-N_2O-N_2 mixtures as a function of nitrogen dilution and initial pressure. The calculated adiabatic constant volume explosion pressures are shown by the solid lines.
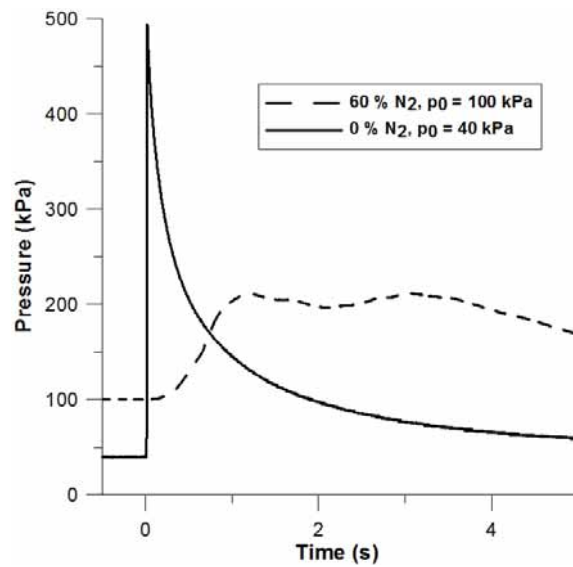
Figure 7: Pressure vs. time for explosions in two H_2-N_2O mixtures with $\phi = 0.3$: one with 60% N_2 dilution and initial pressure of 100 kPa, and the other with no dilution and initial pressure of 40 kPa.
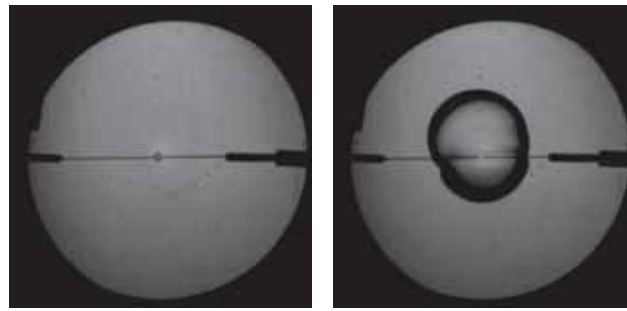
(a) t=0 ms

(b) t=42 ms
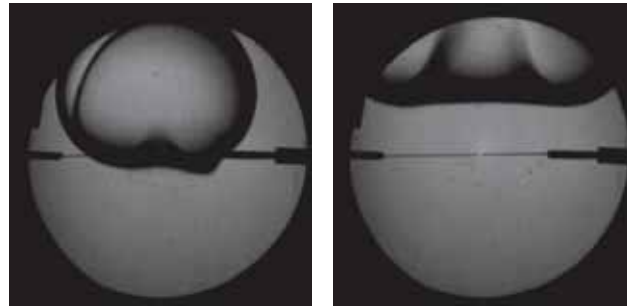
(c) t=109 ms

(d) t=202 ms
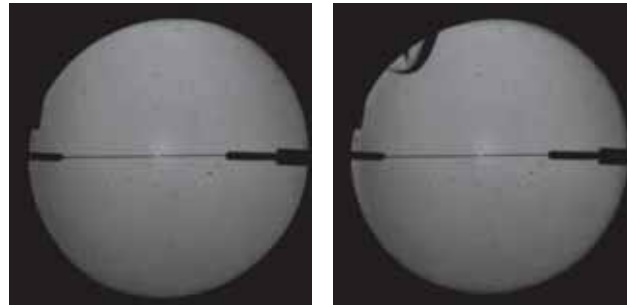
(e) t=332 ms

(f) t=502 ms
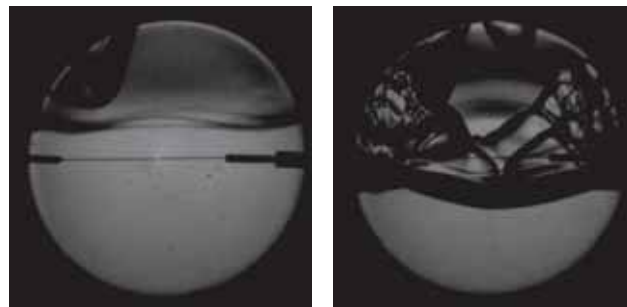
(g) t=600 ms

(h) t=667 ms

Figure 8: Schlieren image sequence showing a buoyant flame in a H_2-N_2O-N_2 mixture with 60% N_2 dilution, $\phi = 0.3$, and 100 kPa initial pressure.

The pressure rise coefficient, K_g, as a function of equivalence ratio for undiluted mixtures at 20 and 40 kPa initial pressure is shown in Figure 9 and given in Table 5 in the Electronic Supplementary Material. The coefficient K_g is calculated as the maximum time derivative of the pressure multiplied by the cubic root of the combustion vessel volume. This parameter allows for comparison of the pressure increase rate, which is a function of vessel volume and other factors and is commonly used [38, 39] for hazard assessment. Due to the digital nature of the pressure data, calculating the maximum time derivative presents some difficulties. A Savitzky-Golay filter with a seventh-order polynomial and 11 data points was used to filter the data and estimate derivatives. The results for K_g depend on the fitting parameters and these values are our best estimates with the uncertainty ranges shown in Figure 9. The value of K_g ranged from 1.5 MPa·m/s for $\phi = 0.15$ ($p_0 = 20$ kPa) to 35 MPa·m/s for $\phi = 0.70$ ($p_0 = 40$ kPa). These values are comparable to the pressure rise coefficients for stoichiometric methane-air (5.5 MPa·m/s) and hydrogen-air (55 MPa·m/s) mixtures [38].
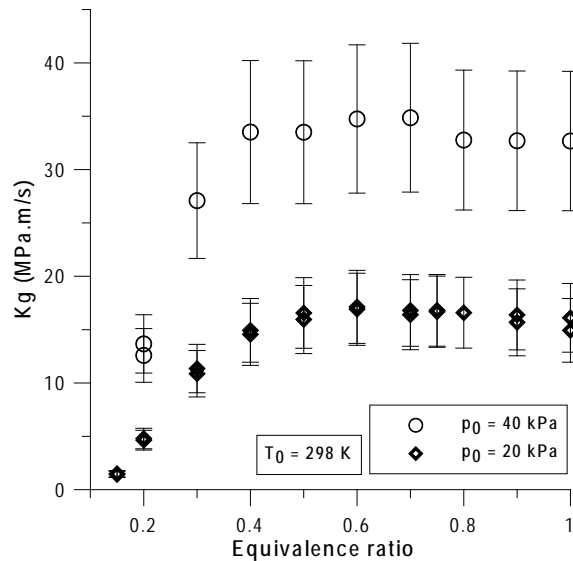

Figure 9: Pressure rise coefficients, K_g, as a function of equivalence ratio for undiluted H_2-N_2O mixtures at initial pressures of 20 and 40 kPa.

Figure 9 shows that the behavior of K_g versus equivalence ratio is different than that of the burning speed. K_g increases strongly with increasing equivalence ratio in the range $\phi = 0.15 - 0.4$. However, for higher equivalence ratios, K_g remains nearly constant at 17 and 35 MPa·m/s for initial pressures of 20 and 40 kPa, respectively. The magnitude of K_g peaks near $\phi = 0.3 - 0.4$, and in order to explain the evolution of K_g, the stability of the flames must be taken into account.

In previous work by Kunz [39], a dimensionless value of K_g was computed to remove the effect of the initial pressure. The dimensionless coefficient, K'_g, is computed using the peak pressure and the laminar burning speed:

$$K'_g = \frac{K_g}{\Delta p_{max} S_L^0} \tag{9}$$

where $\Delta p_{max} = p_{max} - p_0$.

The dimensionless pressure rise coefficient, K'_g, is plotted as a function of equivalence ratio in Figure 10, and the values are also given in Table 5 in the Electronic Supplementary Material. The evolution of K'_g can be explained by the evolution and relative variation of K_g, S_L^0, and p_{max} as a function of equivalence ratio. K_g reaches a quasi-constant value at $\phi = 0.40$, so between $\phi = 0.40$ and $\phi = 1.0$ the K_g values are very comparable. As seen in Figures 2 and 5, the laminar burning speed increases significantly from $\phi = 0.30$ to $\phi = 1.5$. Because of the burning speed variation, the dimensionless K_g value is high for $\phi = 0.3$ and lower for $\phi > 0.40$. Although the peak pressure attains a maximum near $\phi = 0.4$, the relative variations in the range $\phi = 0.30 - 1.0$ are too small (only a few percent) to counterbalance the effect of the burning speed on the value of K'_g. Kunz [39] obtained values of K'_g for hydrogen-, methane-, ethane-, and propane-air mixtures. The dimensionless coefficient was found to range from 4.3 to 48 for the four fuels, with 80% of the data points having a K'_g value between 8 and 16. For the hydrogen-nitrous oxide mixtures studied in the current work, K'_g was found to be significantly larger, ranging from 23 to 106 with 93% of the data points having a K'_g value between 20 and 80.
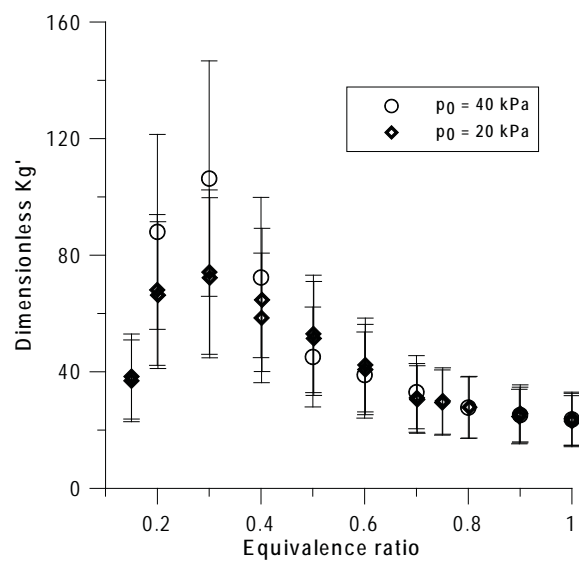
Figure 10: Dimensionless pressure rise coefficients, K'_g, as a function of equivalence ratio for undiluted H_2-N_2O mixtures at initial pressures of 20 and 40 kPa.

Figure 11 shows the Markstein lengths versus equivalence ratio measured from the experiments at 20 kPa initial pressure. All the Markstein lengths were found to be negative. This is expected because in lean mixtures, $L \sim \mathrm{Le} - 1$, where Le is the Lewis number of the deficient reactant, which in this case is H_2. The Lewis number for hydrogen is less than unity, so $L \sim \mathrm{Le} - 1 < 0$ and hence the Markstein lengths are negative. Therefore, according to Equation 1, as the flame propagates and the stretch decreases, the burning speed will also decrease. The Markstein lengths found in this work correspond to Markstein numbers between approximately -0.6 and -1.2, which are smaller than the Markstein numbers found for H_2-air mixtures by Lamoureux et al. [29]. As the equivalence ratio increases from $\phi = 0.15$ to $\phi = 0.40$, the Markstein length increases quickly. However, for higher equivalence ratios ($\phi = 0.4 - 0.7$), the increase in Markstein number is significantly less. These trends found in this work are in good agreement with previous data [21].

Figure 11: Measured Markstein lengths versus equivalence ratio for H_2-N_2O mixtures at 20 kPa initial pressure.

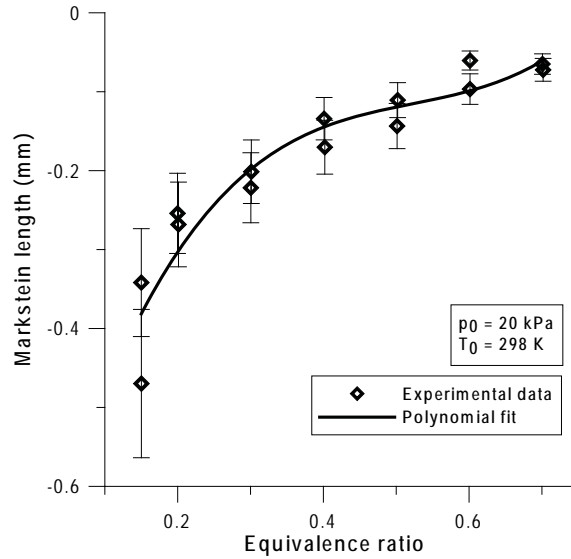In this work it was also observed that because flames in lean H_2-N_2O mixtures are highly unstable, they become cellular at earlier times than flames in mixtures closer to stoichiometric, behavior that was very clear in the schlieren visualization. As cells develop on the flame front, the flame surface increases and the flame can possibly become turbulent. The increase in the flame surface area increases the energy release rate and thus also increases the burning speed. It is interesting to note that in their study of deflagration-to-detonation transition, Liang et al. [12] reported that a flame in an undiluted mixture containing 30% H_2 in N_2O ($\phi = 0.43$) was able to transition to a detonation in a 1.25 m long unobstructed closed tube with initial pressure and temperature of 100 kPa and 298 K. The current experimental results show that lean mixtures have very unstable flame fronts which can enhance flame acceleration, consistent with the findings of Liang et al. [12]. This acceleration can lead to deflagration-to-detonation transition, which poses a severe hazard to the pipe or reservoir structure.

5. Conclusions

In the present study, undiluted and nitrogen-diluted H_2-N_2O mixtures have been characterized through experimental measurements and calculations of the laminar burning speed and explosion pressure. The effects of dilution, equivalence ratio, and pressure on the burning speed were investigated experimentally by varying the nitrogen molar percentage from 0 to 55%, the equivalence ratio from $\phi = 0.15$ to 1.0, and the initial pressure from 20 to 80 kPa. The experiments showed that flames in H_2-N_2O mixtures have burning speeds as high as 350 cm/s and that the flames can be highly unstable. It was also demonstrated that calculations using a detailed chemical mechanism could predict the laminar burning speed to within 10% of the experimental value as long as the mixture was sufficiently far from the lean limit. Burning speeds for higher-pressure conditions (100-300 kPa) were computed for a wide range of H_2-N_2O mixtures. The burning speeds in these mixtures are higher than those for hydrocarbon-air mixtures, and only slightly lower than burning speeds in H_2-O_2, and the mixtures exhibit large expansion ratios on the order of 10 or higher. These high flame burning speeds and large expansions, combined with the

fast onset of cellular instability for lean mixtures, indicate a serious hazard of flame acceleration and deflagration-to-detonation transition in H_2-N_2O mixtures.

References

[1] M. S. Gerber, Legend and legacy: Fifty years of defense production at the hanford site, Tech. Rep. WHC-MR–0293-Rev.2, Westinghouse Hanford Co. (1992).

[2] N. D. Lichtenstein, The hanford nuclear waste site: a legacy of risk, cost, and inefficiency, Nat Resour J 44 (2004) 809–39.

[3] L. A. Mahoney, J. L. Huckaby, S. A. Bryan, G. D. Johnson, Overview of the flammability of gases generated in Hanford waste tanks, Tech. Rep. PNNL-13269, Pac. Northwest Natl. Lab., Richland, Wash. (2000).

[4] K. L. Cashdollar, M. Hertzberg, I. A. Zlochower, C. E. Lucci, G. R. Grenn, R. A. Thomas, Laboratory flammability studies of mixtures of hydrogen, nitrous oxide, and air, Tech. Rep. WHC-SD-WM-ES-219, Pittsburgh Res. Cent. (1992).

[5] R. Mével, F. Lafosse, L. Catoire, N. Chaumeix, G. Dupré, C.-E. Paillard, Induction delay times and detonation cell size prediction of hydrogen-nitrous oxide-argon mixtures, Combust Sci and Technol 180 (2008) 1858–75.

[6] R. Mével, S. Javoy, F. Lafosse, N. Chaumeix, G. Dupré, C.-E. Paillard, Hydrogen-nitrous oxide delay time: Shock tube experimental study and kinetic modelling, Proc Combust Inst 32 (2009) 359–66.

[7] S. Javoy, R. Mével, C.-E. Paillard, A study of N_2O decomposition rate constant at high temperature: Application to the reduction of nitrous oxide by hydrogen, Int J Chem Kinetics 41 (2009) 357–75.

[8] R. Akbar, M. Kaneshige, E. Schultz, J. E. Shepherd, Detonations in H_2-N_2O-CH_4-NH_3-O_2-N_2 mixtures, GALCIT rep. FM97-3, Grad. Aerosp. Lab., Calif. Inst. Tech. (1997).

[9] M. Kaneshige, E. Schultz, U. Pfahl, J. Shepherd, R. Akbar, Detonation in mixtures containing nitrous oxide, Proc. 22nd Int. Symp. Shock Waves 1 (2000) 251–56.

[10] F. Scott, R. V. Dolah, M. Zabetakis, The flammability characteristics of the system H_2-NO-N_2O-air, in: 6th Symp. (Int.) Combust., The Combustion Institute, Pittsburgh, PA, 1957, pp. 540–545.

[11] U. Pfahl, M. Ross, J. Shepherd, Flammability limits, ignition energy, and flame speeds in H_2-CH_4-NH_3-N_2O-O_2-N_2 mixtures, Combust Flame 123 (2000) 140–58.

[12] Z. Liang, J. Karnesky, J. Shepherd, Structural response to reflected detonation and deflagration-to-detonation transition in H_2-N_2O, GALCIT rep. FM2006-003, Grad. Aerosp. Lab., Calif. Inst. Tech. (2006).

[13] E. A. Rodriguez, Pressure-time history for design of hpav vessel and piping subjected to gaseous H_2-N_2O deflagrations, Eng. Rep. GNNA-08-039, Bechtel Natl. Inc. (2008).

[14] P. Gray, S. Holland, D. B. Smith, The effect of isotopic substitution on the flame speeds of hydrogen-oxygen and hydrogen-nitrous oxide flames, Combust Flame 14 (1970) 361–74.

[15] M. J. Brown, D. B. Smith, Aspects of nitrogen flame chemistry revealed by burning velocity model, in: 25th Symp. (Int.) Combust., The Combustion Institute, Pittsburgh, PA, 1994, pp. 1011–18.

[16] P. Gray, R. MacKinven, D. B. Smith, Combustion of hydrogen and hydrazine with nitrous oxide and nitric oxide: Flame speeds and flammability limits of ternary mixtures at sub-atmospheric pressures, Combust Flame 11 (1967) 217–26.

[17] S. Holland, D. T. Jones, P. Gray, Combustion supported by nitrous oxide: Flame speeds and flammability limits in the hydrogen+ethane+nitrous oxide system, Combust Flame 17 (1971) 31–5.

[18] L. S. Kozachenko, G. I. Skachkov, Zh. prikl. mekham.i tekhn. fiz., vol. 2 (1960).

[19] G. Dixon-Lewis, M. Sutton, A. Williams, Stability of hydrogen-nitrous oxide-nitrogen flames on a flat flame burner, Combust Flame 8 (1964) 85–7.

[20] O. A. Powell, P. Papas, C. Dreyer, Laminar burning velocities for hydrogen-, methane-, acetylene-, and propane-nitrous oxide flames, Combust Sci Technol 181 (2009) 917–36.

[21] R. Mével, F. Lafosse, N. Chaumeix, G. Dupré, C.-E. Paillard, Spherical expanding flames in H_2-N_2O-Ar mixtures: Flame speed measurement and kinetic modeling, Int J Hydrogen Energy 34 (2009) 9007–18.

[22] E. Kwon, S. P. Moffett, J. E. Shepherd, A. C. Day, Combustion characteristics of hydrogen as used in a flammable test mixture, int. Conf. Light. Static Electr., paper PPR-48 (2007).

[23] G. I. Sivashinsky, On a distorted flame front as a hydrodynamic discontinuity, Acta Astronautica 3 (1976) 889–918.

[24] M. Matalon, B. J. Matkowsky, Flames as gasdynamic discontinuities, J Fluid Mech 124 (1982) 239–259.

[25] P. Clavin, Dynamic behavior of premixed flame fronts in laminar and turbulent flows, Prog Energy Combust Sci 11 (1985) 1–59.

[26] S. Jerzembeck, M. Matalon, N. Peters, Experimental investigation of very rich laminar spherical flames under microgravity conditions, Proc Combust Inst 32 (2009) 1125–1132.

[27] D. R. Dowdy and D. B. Smith and S. C. Taylor and A. Williams, The use of expanding spherical flames to determine burning velocities and stretch effects in hydrogen/air mixtures, Proc Combust Inst 23 (1990) 325–32.

[28] K. T. Aung, M. I. Hassan, G. M. Faeth, Flame stretch interactions of laminar premixed hydrogen / air flames at normal temperature and pressure, Combust Flame 109 (1997) 1–24

[29] N. Lamoureux, N. Djebaili-Chaumeix, C. Paillard, Laminar flame velocity for H_2-air-He-CO_2 mixtures using the spherical bomb method, Exp Thermal Fluid Sci 27 (2003) 385–93.

[30] T. Dubois, N. Chaumeix, C.-E. Paillard, Experimental and modeling study of n-

propylcyclohexane oxidation under engine-relevant conditions, Energy and Fuels 23 (2009) 2453–2466.

[31] D. Goodwin, Cantera: Object-oriented software for reacting flows, Calif. Inst. Tech., http://sourceforge.net/projects/cantera/ (2005).

[32] R. Mével, Etude de mécanismes cinétiques et des propriétés explosives des mélanges hydrogène-protoxyde d'azote et silane-protoxyde d'azote. application à la sécurité industrielle, Ph.D. thesis, Université d'Orléans (2009).

[33] M. Mueller, R. Yetter, F. Dryer, Kinetic modelling of the $CO/H_2O/O_2/NO/SO_2$ system: Implications for high-pressure fall-off in the $SO_2+O(+M)=SO_3(+M)$ reaction, Int J Chem Kinetics 32 (2000) 317–39.

[34] A. A. Konnov, Development and validation of a detailed reaction mechanism for the combustion of small hydrocarbons, 28th Symp. (Int.) Combust., Abstr. Symp. Pap. p. 317 (2000).

[35] K. Kuo, Principles of Combustion, John Wiley and Sons, Inc., USA, 1986.

[36] S. P. M. Bane, Spark ignition: Experimental and numerical investigation with application to aviation safety, Ph.D. thesis, California Institute of Technology (2010).

[37] S. P. M. Bane, J. E. Shepherd, E. Kwon, A. C. Day, Statistical analysis of electrostatic spark ignition of lean $H_2/O_2/Ar$ mixtures, Int J Hydrogen Energy 36 (2011) 2344–50.

[38] Natl. Fire Prot. Assoc., NFPA 68 standard on explosion protection by deflagration venting (2007).

[39] O. Kunz, Combustion characteristics of hydrogen- and hydrocarbon-air mixtures in closed vessels, Master's thesis, California Institute of Technology (1998).

Tabulated Experimental and Computational Results

Table 1: Laminar burning speeds and Markstein lengths found experimentally and calculated using a 1D flame model for undiluted H_2-N_2O mixtures at 20 kPa initial pressure.

ϕ	p_0 (kPa)	T_0 (K)	V_s^0 (cm/s)	L (mm)	Experimental S_L^0 (cm/s)	Model S_L^0 (cm/s)
0.15	20.00	297.55	199.92	-0.47	18.64	11.80
0.15	20.00	297.85	218.51	-0.34	20.38	11.80
0.20	20.00	294.95	353.17	-0.27	32.74	24.50
0.20	20.00	296.05	352.52	-0.25	32.79	24.50
0.30	20.00	299.75	770.28	-0.20	70.03	61.00
0.30	20.00	299.65	762.82	-0.22	69.86	61.00
0.40	20.00	296.55	1219.52	-0.13	112.57	107.00
0.40	20.00	296.75	1136.63	-0.17	104.92	107.00
0.50	20.00	297.05	1563.53	-0.14	141.55	155.00
0.50	20.00	297.35	1648.17	-0.11	149.22	155.00
0.60	20.00	297.35	2077.62	-0.10	191.36	201.00
0.60	20.00	297.65	2127.68	-0.06	195.11	201.00
0.70	20.00	297.85	2789.10	-0.06	258.25	247.00
0.70	20.00	298.15	2806.40	-0.07	259.85	247.00

Table 2: Laminar burning speeds and Markstein lengths found experimentally and calculated using a 1D flame model for H_2-N_2O-N_2 mixtures with 20-55% N_2 dilution and initial pressures of 20 to 80 kPa.

ϕ	p_0 (kPa)	% N_2	V_s^0 (cm/s)	L (mm)	Experimental S_L^0 (cm/s)	Model S_L^0 (cm/s)
1.00	20	40	923	-0.025	109	111
1.01	20	40	974	0.101	110	111
1.00	20	30	1437	-0.020	159	162
1.00	20	30	1399	-0.050	155	162
1.00	20	20	2070	0.009	213	222
1.00	20	20	2053	-0.005	212	222
1.00	40	50	535	0.071	68	65
1.00	40	50	495	-0.035	62	65
1.00	40	40	926	0.011	105	109
1.00	40	40	919	-0.005	104	109
1.00	40	30	1427	-0.034	154	161
1.00	40	30	1419	-0.017	154	161
1.00	40	20	2022	-0.028	208	218
1.00	40	20	2035	-0.018	209	218
1.00	60	55	321	-0.060	42	45
1.00	60	55	339	0.007	45	45
1.00	60	50	490	-0.049	61	63
1.00	60	50	466	-0.127	58	63
1.00	60	40	883	-0.045	100	107
1.00	60	40	914	-0.010	103	107
1.00	60	30	1393	0.007	148	159
1.00	60	30	1380	0.002	146	159
1.00	60	20	1973	-0.002	200	216
1.00	60	20	1996	0.008	203	216
1.00	80	55	332	-0.009	44	45
1.00	80	55	317	-0.073	41	45
1.00	80	50	498	0.003	62	63
1.00	80	50	459	-0.147	57	63
1.00	80	40	912	-0.002	103	106
1.00	80	40	911	0.013	103	106
1.00	80	30	1419	0.003	151	157
1.00	80	30	1381	-0.004	148	157

Table 3: Laminar burning speeds calculated using the mechanism of Mueller et al. [1] for stoichiometric H_2-N_2O-N_2 mixtures with varying N_2 dilution.

N_2 Mole Fraction	S_L^0 (cm/s)
0	329
0.05	297
0.1	265
0.15	238
0.2	209
0.25	179
0.3	151
0.35	125
0.4	103
0.45	80
0.5	60
0.55	43
0.6	28
0.65	15
0.7	9.6

Table 4: Laminar burning speeds calculated using the mechanism of Mueller et al. [1] for undiluted H_2-N_2O mixtures at initial pressures of 100, 200, and 300 kPa.

	S_L^0 (cm/s)		
ϕ	$p_0 = 100$ kPa	$p_0 = 200$ kPa	$p_0 = 300$ kPa
0.11	4.0	4.0	4.0
0.18	12	11	11
0.25	32	27	27
0.33	67	61	55
0.43	115	109	99
0.54	154	154	147
0.67	220	211	202
0.82	275	268	261
1.00	329	323	316
1.22	363	354	347
1.50	367	358	345
1.86	344	335	327
2.33	297	292	281
3.00	230	223	216
4.00	151	143	133

Table 5: Peak combustion pressures and values of K_g and K_g' for undiluted H_2-N_2O mixtures at initial pressures of 20 and 40 kPa.

ϕ	p_0 (kPa)	T_0 (K)	p_{max} (kPa)	K_g (MPa·m/s)	K_g'
0.15	20	298	219	1.49	36.91
0.15	20	298	220	1.43	38.38
0.20	20	296	235	4.79	68.08
0.20	20	295	234	4.64	66.31
0.30	20	300	239	11.35	74.20
0.30	20	300	235	10.87	72.28
0.40	20	297	241	14.56	58.48
0.40	20	297	240	14.93	64.66
0.50	20	297	233	15.95	53.01
0.50	20	297	236	16.56	51.43
0.60	20	297	231	17.13	42.33
0.60	20	298	233	16.91	40.77
0.70	20	298	228	16.80	31.04
0.70	20	298	228	16.40	30.49
0.75	20	296	228	16.68	29.44
0.75	20	296	226	16.81	29.97
0.80	20	296	224	16.59	27.84
0.90	20	297	221	15.69	24.64
0.90	20	297	221	16.38	25.73
1.00	20	297	219	16.11	23.92
1.00	20	298	211	14.93	23.05
0.20	40	295	483	12.58	88.00
0.30	40	297	495	27.09	106.29
0.40	40	297	490	33.52	72.35
0.50	40	298	482	33.50	45.09
0.60	40	299	476	34.75	38.89
0.70	40	298	469	34.86	33.00
0.80	40	299	461	32.77	27.71
0.90	40	299	454	32.70	25.15
1.00	40	299	449	32.68	23.64

References

[1] M. Mueller, R. Yetter, F. Dryer, Kinetic modelling of the $CO/H_2O/O_2/NO/SO_2$ system: Implications for high-pressure fall-off in the $SO_2+O(+M)=SO_3(+M)$ reaction, Int J Chem Kinetics 32 (2000) 317–39.